
[View Journal Online](#)
[View Article Online](#)

Synthesis, crystal structure, DFT/HF, Hirshfeld surface, and molecular docking analysis of 4-(*tert*-butyl)-4-nitro-1,1-biphenyl

Neha Kumari ¹, Ruchika Sharma ¹, Archana Akaram Yadav ², Sandeep Ashok Sankpal ², Jayakumar Mohan Raj ³, Saminathan Murugavel ³ and Rajni Kant ^{1,*}

¹ Department of Physics, University of Jammu, Jammu Tawi-180006, Jammu and Kashmir, India

² Department of Chemistry, Shivaji University Kolhapur-416004, Maharashtra, India

³ Department of Physics, Thanthai Periyar Government Institute of Technology, Vellore-632002, Tamil Nadu, India

* Corresponding author at: Department of Physics, University of Jammu, Jammu Tawi-180006, Jammu and Kashmir, India.

e-mail: rkant.ju@gmail.com (R. Kant).

RESEARCH ARTICLE



doi: 10.5155/eurjchem.14.1.90-98.2386

Received: 13 December 2022

Received in revised form: 10 January 2023

Accepted: 12 January 2023

Published online: 31 March 2023

Printed: 31 March 2023

KEYWORDS

X-ray diffraction
 Molecular docking
 Hartree-Fock method
 Single crystal structure
 Density functional theory
 Hirshfeld surface analysis

ABSTRACT

4-(*tert*-Butyl)-4-nitro-1,1-biphenyl has been synthesized, and its structure has been characterized by using some spectroscopic and single-crystal X-ray diffraction techniques. It crystallizes in a monoclinic crystal system with space group $P2_1/n$ and unit cell parameters: $a = 6.4478(3) \text{ \AA}$, $b = 9.2477(4) \text{ \AA}$, $c = 23.4572(9) \text{ \AA}$, $\beta = 95.114(4)^\circ$, $V = 1393.11(10) \text{ \AA}^3$, $Z = 4$. The molecular structure has been solved by using the intrinsic phasing method. The crystal structure is stabilized by C-H...O interactions. Computational studies were performed using density functional theory (DFT) and Hartree-Fock (HF) methods. The optimized geometry obtained from DFT and HF in the gas phase was compared with solid-phase experimental data retrieved from single-crystal X-ray diffraction results. Frontier molecular orbitals, such as the HOMO/LUMO energy gap, the molecular electrostatic potential, and Mulliken atomic charges, have been investigated. The HOMO LUMO energy gap of 3.97 eV indicates that the molecule is soft and highly reactive. The Hirshfeld surface analysis and their associated fingerprint plots have been used to quantitatively validate the interactions. Further insilico molecular docking studies have been performed with the molecular target Type-II topoisomerase (PDB ID: 1J1J) and their results suggest that 4-(*tert*-butyl)-4-nitro-1,1-biphenyl could be considered an anticancer drug.

Cite this: *Eur. J. Chem.* 2023, 14(1), 90-98

Journal website: www.eurjchem.com

1. Introduction

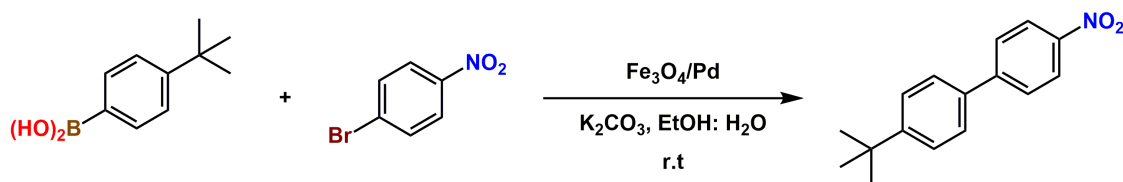
Biphenyls are an important aromatic hydrocarbon that serves as an important structural analogue and are widely used in the synthesis of various compounds [1]. Biphenyls and their derivatives are well-known and are more widely studied because of their many chemical and biological properties. In the UV region, they exhibit strong absorption but only weak fluorescence [2]. It serves as a central building block for basic liquid crystal and fluorescent layers in OLEDs [3,4]. The ability of biphenyls to undergo chemical changes to form substituted biphenyls has many biological and pharmaceutical applications, including anti-inflammatory, antimicrobial, antifungal, anti-diabetic, anti-tumor, and anticancer properties [5-9]. The search for new and efficient pharmaceuticals is a constant struggle for medicinal chemists, in view of the fact that the new compounds synthesized by various standard methods should be safe, effective, and have fewer side effects. Some functional groups, viz. $-\text{NO}_2$ is an efficient scaffold for bioactive molecules that have a wide spectrum of activities [10-16]. The *tert*-butyl group is a common group present in many drugs across different therapeutic classes. Despite its simple bulky

structure, *tert*-butyl groups have unique properties and can serve to change or increase specificity, or act as steric shields to increase the stability of compounds containing chemically or enzymatically susceptible groups [17]. Therefore, a biphenyl having $-\text{NO}_2$ and *tert*-butyl group has been undertaken for the synthesis and structural characterization, so as to know about their possible biological activities and some other important findings.

The 4-(*tert*-butyl)-4-nitro-1,1-biphenyl (4-TBNB) compound has been synthesized and its structure has been characterized using FT-IR, ^1H NMR and ^{13}C NMR techniques. The chemical structure was validated by the single-crystal X-ray diffraction method, and an optimized structure was obtained using DFT and Hartree-Fock (HF) approaches. A wide range of calculations using DFT helps develop a close relationship between theoretical and experimental data by giving clues related to molecular geometry, electrical, and spectroscopic properties [18]. Theoretical computational techniques have become very reliable in predicting the properties of molecules with great precision [19-21].

Table 1. Crystal data and structure refinement for 4TBNB.

CCDC No.	2208826
Empirical formula	C ₁₆ H ₁₇ NO ₂
Formula weight (g/mol)	255.30
Temperature (K)	293(2)
Crystal system	Monoclinic
Space group	P2 ₁ /n
a, (Å)	6.4478(3)
b, (Å)	9.2477(4)
c, (Å)	23.4572(9)
α (°)	90
β (°)	95.114(4)
γ (°)	90
Volume (Å ³)	1393.11(10)
Z	4
ρ _{calc} (g/cm ³)	1.217
μ (mm ⁻¹)	0.080
F(000)	544.0
Crystal size (mm ³)	0.35 × 0.1 × 0.1
Radiation	Mo Kα (λ = 0.71073)
2θ range for data collection (°)	6.428 to 52.734
Index ranges	-7 ≤ h ≤ 8, -11 ≤ k ≤ 11, -29 ≤ l ≤ 28
Reflections collected	12104
Independent reflections	2744 [R _{int} = 0.0328, R _{sigma} = 0.0317]
Data/restraints/parameters	2744/0/176
Goodness-of-fit on F ²	1.066
Final R indexes [I ≥ 2σ (I)]	R ₁ = 0.0542, wR ₂ = 0.1489
Final R indexes [all data]	R ₁ = 0.0919, wR ₂ = 0.1739
Largest diff. peak/hole (e.Å ⁻³)	0.28/-0.17

**Figure 1.** Schematic representation of the synthesis of the compound 4TBNB.

Therefore, DFT and HF calculations have been used to optimize the given structure, and their optimized parameters (bond length and angles) were correlated with the experimental X-ray single-crystal data. Furthermore, molecular docking simulations were used to predict the biological activity of 4TBNB with Type-II topoisomerase (protein) against the anticancer drug. Type-II topoisomerases (PDB ID: 1JII) are ubiquitous enzymes that play essential roles in a number of critical DNA processes [22]. They are the cytotoxic targets for a number of highly successful anticancer agents and represent some of the most successful chemotherapeutic drugs currently used for the treatment of human malignancies. Despite the significance of topoisomerase II α and II β to the survival of human cells and the efficacy of cancer chemotherapy, considerable evidence indicates that these enzymes have significant genotoxic effects and can trigger specific leukemic chromosomal translocations [23].

2. Experimental

2.1. Instrumentation

The ¹H NMR and ¹³C NMR spectra were obtained using a Bruker high-resolution NMR spectrometer of frequency 400-100 MHz with CDCl₃ as a solvent. Fourier transform infrared (FT-IR) spectra were recorded in the range of 400-4000 cm⁻¹ on a Bruker IR spectrophotometer.

2.2. Synthesis

Fe₃O₄/Pd (10 mg) was placed in a 25 mL round bottom flask. Then 1 mmol of 1-bromonitrobenzene, 1.1 mmol of 4-*tert*-butyl phenylboronic acid, and 0.276 mg of K₂CO₃ (2 mmol) in 3 mL of water: ethanol mixture (1:1) were added to the flask. The

mixture was then stirred at 40 °C. The reaction was monitored by TLC. After the reaction was completed, 5 mL of ethanol was added and the catalyst was removed using an external magnet. In addition, purification was achieved by simple recrystallisation. The 4-(*tert*-butyl)-4-nitro-1,1-biphenyl product was dissolved in ethanol and the solution was kept at room temperature for 3-4 days to obtain single crystals. The schematic representation of the synthesis of the compound 4TBNB is shown in Figure 1.

4-(*tert*-Butyl)-4-nitro-1,1-biphenyl: Color: Yellow. Yield: 88%. M.p.: 112-114 °C. FT-IR (KBr, ν, cm⁻¹): 2951-2865 (Aromatic C-H), 1592 (C=C), 1506 (-NO₂), 1334 (ter. C-H), 833 (C-H bend.). ¹H NMR (400 MHz, CDCl₃, δ, ppm): 1.34 (s, 9H, -CH₃), 7.71-7.50 (t, 6H, ArH), 8.26 (s, 2H, ArH). ¹³C NMR (100 MHz, CDCl₃, δ, ppm): 31.25 (3C, CH₃), 34.71 (1C, -C-CH₃), 124.10 (2C, Ar-C), 126.14 (2C, Ar-C), 127.05 (2C, Ar-C), 127.57 (2C, Ar-C), 135.79 (1C, Ar-C), 146.84 (1C, C-NO₂), 147.47 (1C, C-Ar-(CH₃)₃), 152.27 (1C, C-(CH₃)₃).

2.3. Crystal structure determination and refinement

The X-ray intensity data for a well-defined single crystal of size 0.30×0.10×0.10 mm³ were collected on the Supernova HyPix3000 X-ray diffractometer. The measurements were carried out at 293(2) K with monochromatic Mo-K α radiation (λ = 0.71073 Å). The crystal structure has been solved by intrinsic phasing of SHELXT [24] and refined by full-matrix least-squares refinement method based on F² with SHELXL [25] in the OLEX 2 software [26]. The precise crystallographic data are summarized in Table 1. All non-hydrogen atoms were located from E-map and were refined anisotropically. After several cycles of refinement, the final difference Fourier map shows the peak of no chemical significance, and the final residual factor converges to 0.0503.

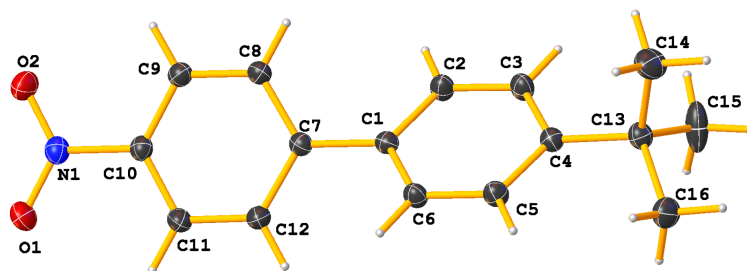
Table 2. Bond lengths and angles for 4TBNB.

Atom	Atom	X-ray (Å)	DFT (Å)	HF (Å)	Atom	Atom	X-ray (Å)	DFT (Å)	HF (Å)		
C1	C7	1.486(3)	1.481	1.487	C4	C5	1.381(3)	1.404	1.388		
C1	C2	1.383(3)	1.399	1.392	C4	C3	1.381(3)	1.399	1.396		
C1	C6	1.382(3)	1.403	1.385	C4	C13	1.529(3)	1.538	1.538		
N1	C10	1.471(3)	1.474	1.463	C12	C11	1.372(3)	1.388	1.393		
N1	O1	1.215(2)	1.226	1.188	C9	C8	1.373(3)	1.387	1.381		
N1	O2	1.221(2)	1.226	1.188	C5	C6	1.382(3)	1.388	1.385		
C10	C9	1.368(3)	1.391	1.381	C2	C3	1.379(3)	1.393	1.379		
C10	C11	1.368(3)	1.391	1.381	C13	C14	1.521(3)	1.539	1.542		
C7	C12	1.391(3)	1.405	1.393	C13	C16	1.542(3)	1.546	1.536		
C7	C8	1.383(3)	1.405	1.393	C13	C15	1.511(3)	1.546	1.542		
Atom	Atom	Atom	X-ray (°)	DFT (°)	HF (°)	Atom	Atom	Atom	X-ray (°)	DFT (°)	HF (°)
C2	C1	C7	121.16(19)	121.23	121.11	C11	C12	C7	121.6(2)	121.27	121.06
C6	C1	C7	121.85(18)	121.31	121.25	C10	C9	C8	119.1(2)	118.84	118.76
C6	C1	C2	116.99(18)	117.45	117.64	C9	C8	C7	121.3(2)	121.27	121.06
O1	N1	C10	118.3(2)	117.75	117.67	C10	C11	C12	118.7(2)	118.84	118.77
O1	N1	O2	123.2(2)	124.50	124.65	C4	C5	C6	122.1(2)	121.82	121.64
O2	N1	C10	118.4(2)	117.75	117.67	C3	C2	C1	120.9(2)	121.21	120.95
C9	C10	N1	119.1(2)	119.20	119.12	C2	C3	C4	122.8(2)	121.61	121.87
C11	C10	N1	119.4(2)	119.21	119.12	C4	C13	C16	112.28(19)	112.33	112.28
C11	C10	C9	121.55(19)	121.58	121.76	C14	C13	C4	108.92(19)	109.43	109.50
C12	C7	C1	120.86(19)	120.90	120.72	C14	C13	C16	106.4(2)	108.20	108.02
C8	C7	C1	121.46(18)	120.91	120.69	C15	C13	C4	110.39(19)	109.44	109.47
C8	C7	C12	117.68(18)	118.18	118.58	C15	C13	C14	110.7(3)	109.37	109.49
C5	C4	C13	122.89(19)	123.04	123.19	C15	C13	C16	108.2(2)	108.17	108.03
C3	C4	C5	115.82(18)	116.84	116.72	C5	C6	C1	121.40(19)	121.03	121.16
C3	C4	C13	121.27(19)	120.12	120.08						

Table 3. Hydrogen bond geometry of 4TBNB*.

D-H...A	d(D-H) (Å)	d(H...A) (Å)	d(D...A) (Å)	∠D-H...A (°)
C14-H14A...O1 ⁱ	0.96	2.58	3.4451	150

* Symmetry code (i) = 1/2+x, 1/2-y, 1/2+z.

**Figure 2.** The ORTEP diagram of 4TBNB shows the atomic labelling scheme with 50% ellipsoidal probability.

The geometrical calculations were performed using the PLATON [27] and PARST [28] software. ORTEP and molecular packing diagrams were generated using MERCURY [29] software.

2.4. Computational details

Density functional theory (DFT/B3LYP) [30] and Hartree Fock (HF) calculations were performed with the 6-311++G(d,p) basis set in the gas phase using Gaussian 09W software [31]. DFT level calculations were performed with Beck's three-parameter hybrid functional using the Lee-Yang-Parr correlation functional (B3LYP). For comparison of geometrical parameters, optimization has been done with HF and DFT methods. The optimized structure obtained by DFT (B3LYP) has been used to calculate the highest occupied molecular orbital (HOMO) and the lowest unoccupied molecular orbital (LUMO), energy gap, molecular electrostatic potential, and Mulliken charges. Mulliken charges calculated by the DFT and HF methods were also compared. The Gaussian 09W programme and the GaussView 6.0 software [32] have been used to draw the input molecule. The Hirshfeld surfaces and 2D fingerprint plots were generated using Crystal Explorer (21.5) [33]. The molecular docking study has been performed using AutoDock Vina software [34] and the target protein Type-II topoisomerase (PDB ID: 1JII) file was downloaded from the RCB protein data bank [35]. Discovery Studio 4.1 Visualizer software [36] has

been used to visualize and analyze the predicted docking pose of ligand-protein interactions.

3. Results and discussion

3.1. Molecular geometry

The computed structure with thermal displacement ellipsoids drawn at a 50% probability level is depicted in Figure 2 (ORTEP). The structure contains two rings connected through a bridging bond C1-C7 = 1.49 Å and this value is similar to some analogous structures [37,38]. The optimized parameters (bond lengths and bond angles) obtained from DFT/B3LYP and HF with 6-311 ++ G(d,p) are compared with the experimental SCXRD data (Table 2). The optimized structural parameters, by and large, agree well with the corresponding experimental values, but with some insignificant variations observed in the bond length (C13-C15) and bond angle (O1-N1-O2 and C14-C13-C16). The magnitude of torsion around C2-C1-C7-C8 is 36.67°, which is comparable with the theoretical value. The dihedral angle between the two benzene rings is 37.03°, which is consistent with some similar structures [39,40]. There exists an intermolecular hydrogen bond of type C14-H14A...O1 (Table 3). The molecular structure exhibits two short ring Cg...Cg (π - π) interactions and their details are given in Table 4. The molecular packing with C-H...O and π - π interactions along the *a*-axis is shown in Figure 3.

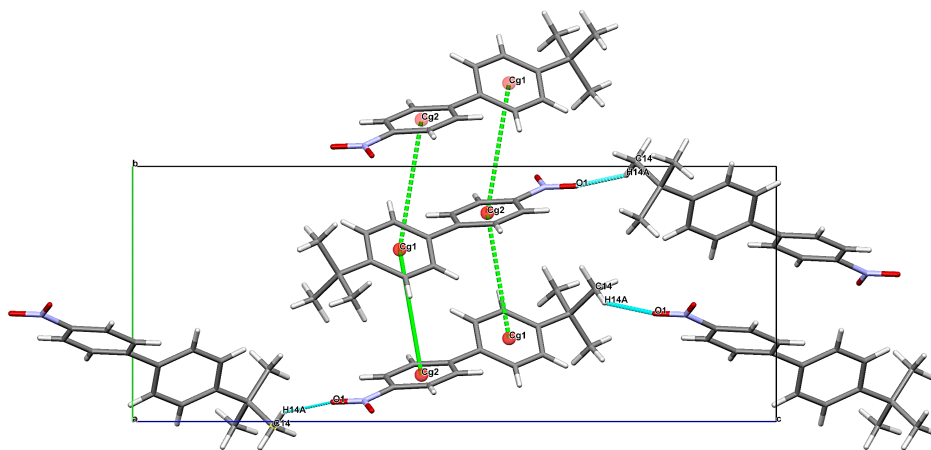
Table 4. π - π interactions involved in 4TBNB.

Cg1	Cg2	Cg1...Cg2	α (°)	β (°)	γ (°)	Cg1 (Å)	Cg2 (Å)
Cg1	Cg2 ⁱ	4.6084(12)	36.96(10)	51.6	17.6	4.3934(8)	2.8614(8)
Cg1	Cg2 ⁱⁱ	4.7740(12)	36.96(10)	45.2	26.4	4.2756(8)	3.3617(8)

* Symmetry codes: (i) -x, -y, -z; (ii) -x, 1-y, -z. Cg1: C1-C2-C3-C4-C5-C6, Cg2: C7-C8-C9-C10-C11-C12.

Table 5. Chemical reactivity parameters and HOMO LUMO energies of 4TBNB.

Parameters	Formula	Value
HOMO energy	E_H	-6.81 eV
LUMO energy	E_L	-2.84 eV
Energy gap	$\Delta E = E_H - E_L $	3.97 eV
Ionization potential	$I = -E_H$	6.81 eV
Electron affinity	$A = -E_L$	2.84 eV
Chemical hardness	$\eta = \Delta E/2$	1.98 eV
Chemical potential	$\mu = -\chi$	-4.82 eV
Electronegativity	$\chi = (I + A)/2$	4.82 eV
Chemical softness	$\sigma = 1/2\eta$	0.25 eV ⁻¹
Global electrophilicity	$\omega = \mu^2/2\eta$	5.86 eV

**Figure 3.** Molecular packing showing the intermolecular hydrogen bonding C-H...O interaction, and π - π interactions in 4TBNB along the *a*-axis.

3.2. Frontier molecular orbital analysis (FMO)

Frontier molecular orbitals (HOMO and LUMO) are a highly effective parameter for finding the chemical reactivity of compounds in quantum chemistry [41]. FMO calculations have been performed using the DFT (B3LYP/6-311++G(d,p)) basis set and the energies of the HOMO and LUMO orbitals are -2.8381 and -6.8060 eV, respectively (Figure 4). The energy gap between HOMO and LUMO is 3.97 eV and refers to a soft molecule, less stable and easy transfer of electrons from HOMO to LUMO (Figure 4). A small value of the orbital energy gap represents the molecule as soft, unstable, and chemically reactive, while a large value of the orbital energy gap represents the molecule as hard, stable, and chemically less reactive [42]. The chemical reactivity parameters of the molecule, such as the chemical softness (σ), chemical potential (μ), electrophilicity index (ω), and chemical hardness (η) have been calculated using the energies of the HOMO and LUMO orbitals using the Koopman theorem (Table 5) [43]. Ionization potential (I) represents the electron-donating power of a molecule, whereas the electron affinity (A) represents the ability of a molecule to accept the electron. Hardness (η) is a measure for resistance to deformation or change, whereas softness (σ) is the reciprocal of hardness. Electronegativity (χ) is the tendency of an atom in a molecule to attract shared electrons. The chemical potential (μ) of the molecule is expressed as $\mu = -\chi$. Electrophilicity (ω) specifies the electrophilic power of a molecule [44].

3.3. Molecular electrostatic potential

The molecular electrostatic map (MEP) is related to the electronic density and is a useful visual descriptor to determine

the sites of electrophilic and nucleophilic reactions in studies of biological identification, as well as hydrogen bond interactions [45,46]. The negative region (red) of MEP refers to electrophilic reactivity, whereas the positive portion (blue) refers to nucleophilic reactivity, and the green colour indicates the neutral potential. The MEP map of 4TBNB is shown in Figure 5, in which the blue region over the hydrogen atoms indicates an electron-deficient site (nucleophilic reactivity) while the red region around the O1 and O2 atoms indicates an electron-rich site (electrophilic reactivity) that results in the formation of C-H...O interactions. Molecular electrostatic potential (MEP) map is useful for molecular docking analysis, as it helps identify binding sites on the receptor and understand the interactions that occur between the ligand and the receptor [47]. Since the electronegativity of oxygen atoms O1 and O2 is quite high, it is possible that amino acids in proteins may interact with these electronegative atoms, thus making molecular docking studies more useful.

3.4. Mulliken charges

Atomic charges have a great impact on the electrical properties and reactivity of molecules. Therefore, estimating Mulliken atomic charges is essential in quantum chemical calculations for molecular systems [48]. The Mulliken atomic charge distributions of the optimized structure were calculated using the two methods DFT/B3LYP/6-311++G(d,p) and HF/6-311++G(d,p) levels in the gas phase (Figure 6). The carbon atoms (C1, C4, C7, and C13) in the case of both DFT and HF methods possess a positive charge, while the nitrogen, oxygen, and the remaining carbon atoms exhibit a negative charge.

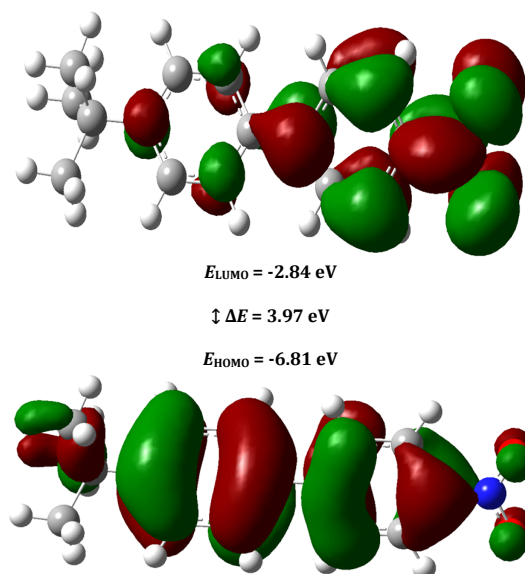


Figure 4. HOMO LUMO energy gap of 4TBNB.

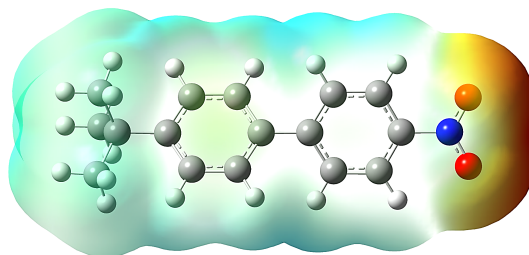


Figure 5. Molecular electrostatic potential map of 4TBNB.

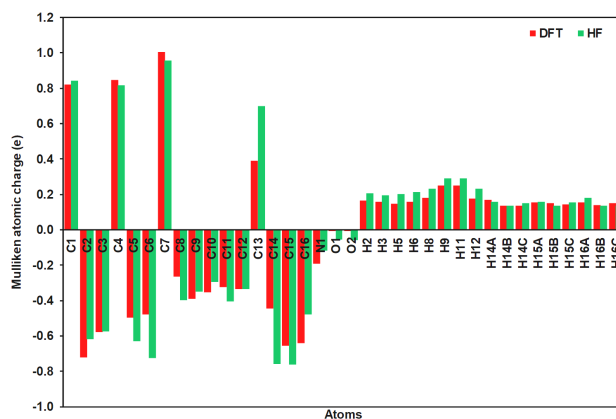


Figure 6. Mulliken atomic population of 4TBNB.

The maximum positive charge is on the C7 atom for both the DFT and HF methods. Moreover, all hydrogen atoms have positive charges, and the charge value increases as we shift from DFT to HF.

3.5. Hirshfeld surface analysis

The Hirshfeld surface analysis (HS) is a powerful tool for calculating and visualizing intermolecular interactions. The HS mapped over d_{norm} is depicted in Figure 7. The bright red spots that appear on the HS indicate the existence of short hydrogen bond interactions due to C-H...O contact (C14-H14A...O1) (shorter than the van der Waals radii). The Hirshfeld surface

plotted over the shape index and curvedness gives more details about the shape and molecular packing in crystals. The shape index map (Figure 7) of the given compound was generated in the range of -1 to 1 Å. The complementary red and blue triangles on the benzene ring of the shape index plot represent the π - π interaction in the crystal structure. The curvedness map (Figure 7) was generated in the range -4 to 4 Å. The flat regions around the benzene ring show the presence of π - π stacking in the given compound.

The two-dimensional fingerprint plots [49] showing the percentage contributions of different intermolecular interactions in the crystal structure are presented in Figure 8.

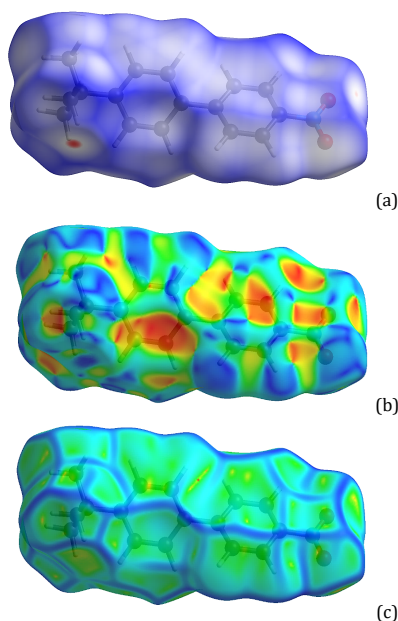


Figure 7. (a) Hirshfeld surface mapped over d_{norm} , (b) Shape index plot, and (c) Curvedness plot of 4TBNB.

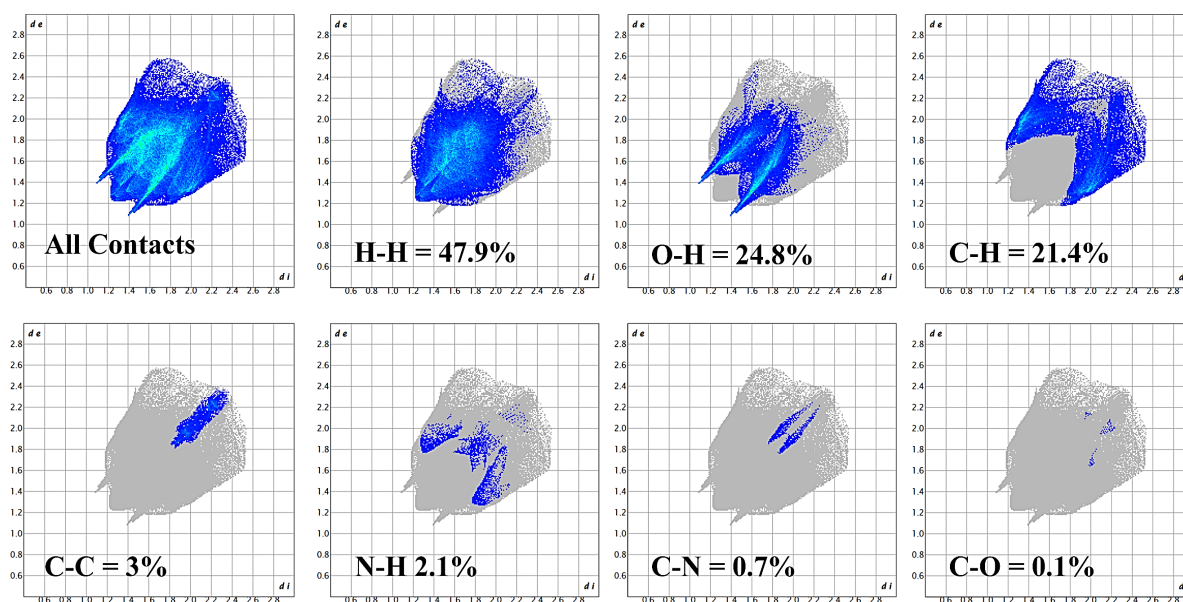


Figure 8. 2D fingerprint plots of 4TBNB.

The $O\cdots H/H\cdots O$ contacts corresponding to the $C\cdots O$ interactions have two sharp symmetric spikes on the fingerprint plot (Figure 8) and contribute 24.8% to the total Hirshfeld area. However, the $H\cdots H$ contacts contribute 47.9% (maximum contribution) and the contribution of $C\cdots H/H\cdots C$ and $C\cdots C$ contacts is 21.4 and 3%, respectively. Crystal Explorer 21.5 software [33] has been used to calculate the voids and their volume in the crystal. The volume of voids is 152.10 \AA^3 and the surface area is 565.29 \AA^2 . Therefore, the percentage of void volume calculated in the crystal 4TBNB is 10.91%, Figure 9 indicates the occurrence of a densely packed molecular structure [50].

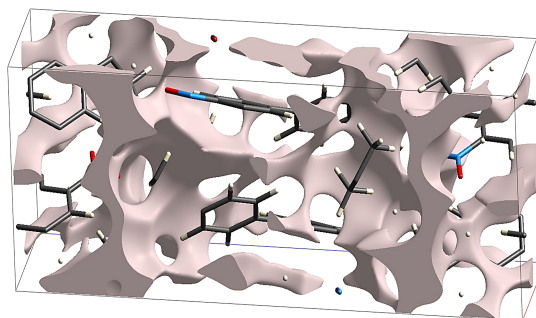
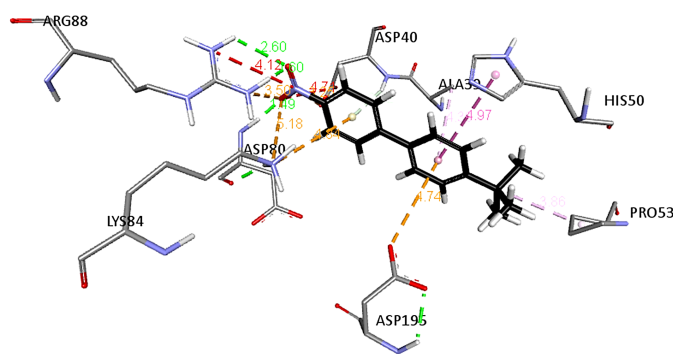
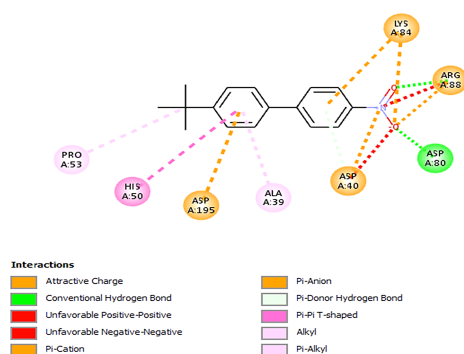
3.6. Molecular docking

The molecular docking is a key tool in drug discovery and molecular modelling applications. The reliability of this

technique depends on the accuracy of the adopted scoring function, which can be used to determine the binding mode and site of a ligand to predict the binding affinity and identification of the potential drug leads for a given protein target. The three-dimensional binding poses and the two-dimensional binding interaction of 4TBNB at the binding site of the 1JJJ enzyme are shown in Figures 10 and 11, respectively. The 4TBNB-1JJJ complex is stabilized by three conventional hydrogen bonds, one π -donor hydrogen bond, five electrostatic bonds, and three hydrophobic bond interactions, respectively (Table 6). The three conventional hydrogen bonds that exist between the donor hydrogen atom of the residues ASP80 and ARG88 interact with the oxygen atom of the 4TBNB at a distance of 1.49 and 1.60 Å, respectively. Furthermore, the π -donor hydrogen bond occurs between the donor hydrogen atom of the residue ASP40 and the benzene ring of the ligand at a distance of 2.92 Å.

Table 6. Binding energy, hydrogen bond, electrostatic and hydrophobic contacts of 4-(*tert*-butyl)-4-nitro-1,1-biphenyl with 1JJ.

Inhibitor	Binding energy, Kcal/mol	Interactions	Distance, Å	Bonding	Bonding types
4TBNB	-7.2	ASP80 [NH...O]	1.49	Hydrogen	Conventional hydrogen bond
		ARG88 [H...O]	1.60	Hydrogen	Conventional hydrogen bond
		ARG88 [H...O]	2.60	Hydrogen	Conventional hydrogen bond
		LYS84 [N...O]	5.18	Electrostatic	Attractive charge
		ARG88 [NH...O]	3.50	Electrostatic	Attractive charge
		ASP40 [O...π]	3.24	Electrostatic	Attractive charge
		LYS84 [N...π]	4.84	Electrostatic	π-Cation
		ASP195 [O...π]	4.73	Electrostatic	π-Sigma
		ASP40 [HN...π]	2.92	Hydrogen bond	π-Donor hydrogen bond
		HIS50 [π...π]	4.97	Hydrophobic	π-π T-shaped
		PRO53 [π...C]	3.86	Hydrophobic	Alkyl
		ALA39 [C...π]	4.30	Hydrophobic	π-Alkyl

**Figure 9.** Crystal void of 4TBNB.**Figure 10.** 3D binding interaction of 4-(*tert*-butyl)-4-nitro-1,1-biphenyl with PDB ID: 1JJ binding site.**Figure 11.** 2D binding interaction of 4-(*tert*-butyl)-4-nitro-1,1-biphenyl with PDB ID: 1JJ binding site.

Three electrostatic interactions (attractive charge) are exhibited in the docking complex that has bonded with nitrogen and oxygen atoms of the active amino acids LYS84, ARG88, and ASP40 at a distance of 5.18, 3.50 and 3.24 Å, respectively. The fourth electrostatic interaction (π-Cation) is exhibited by the six-membered ring of the ligand and has bonded to the nitrogen and oxygen atoms of the active amino acid LYS84 at a distance of 4.84 Å. The last electrostatic interaction (π-Sigma) is

observed between the oxygen atom of ASP195 and the benzene ring atom of the ligand at a distance of 4.73 Å. As evident from Table 6, π-donor hydrogen bond is observed. The hydrophobic interaction (π-π T-shaped) exists between the compound and the HIS50 protein of the six-membered ring at a distance of 4.97 Å. The alkyl hydrophobic interaction occurs by bonding between the carbon atoms of the ligand and the benzene ring of the active enzyme PRO53 at a distance of 3.86 Å. The π-alkyl of

the hydrophobic interaction is bonded between the carbon atom of the active enzyme ALA39 and the benzene ring of the ligand at a distance of 4.30 Å. The binding energy score (-7.2 kcal/mol) for 4-(*tert*-butyl)-4-nitro-1,1-biphenyl and Type II topoisomerase indicates that the 4TBNB molecule may act as a potent anticancer drug.

4. Conclusions

In the present work, we have synthesized and grown single crystals of 4TBNB. The structure has been determined by FT-IR, NMR, SC-XRD, and DFT/HF techniques. The structure crystallizes in the monoclinic crystal system having the space group $P2_1/n$. The theoretical calculations performed by the DFT and HF methods show a good correlation between the observed and calculated values. The crystal structure is stabilized by intermolecular C-H...O and weak $\pi\cdots\pi$ interactions. The energy gap between HOMO and LUMO is 3.97 eV, indicating that the molecule is soft and chemically reactive, allowing easy transfer of electrons from HOMO to LUMO. Molecular electrostatic potential and Mulliken charge analysis revealed the electrophilic and nucleophilic reactivity of the molecule. The red spots on the d_{norm} of Hirshfeld surface confirm the existence of C-H...O interaction, while the curvedness plot indicates the moderate stacking in the crystal structure, which confirms the presence of $\pi\cdots\pi$ interactions. The results of fingerprint plot analysis show that the major contribution to the total Hirshfeld surface area is from H-H contacts (47.9%). The molecular docking investigation shows a good binding score of 4TBNB with Type II topoisomerase, and this indicates that 4TBNB may be regarded as an active and potent anticancer drug.

Acknowledgements

Rajni Kant is thankful to the University of Jammu for funding under the Rashtriya Uchchatar Shiksha Abhiyan (RUSA) 2.0 project of the Government of India.

Supporting information

CCDC-2208826 contains the supplementary crystallographic data for this article. These data can be obtained free of charge via <https://www.ccdc.cam.ac.uk/structures/>, or by e-mailing data_request@ccdc.cam.ac.uk, or by contacting The Cambridge Crystallographic Data Centre, 12 Union Road, Cambridge CB21EZ, UK; Fax: +44 (0)1223-336033.

Disclosure statement

Conflict of interest: The authors declare that they have no conflict of interest. Authors' contributions: All authors contributed equally to this work. Ethical approval: All ethical guidelines have been adhered to. Sample availability: A sample of the compound is available from the author.

CRedit authorship contribution statement

Conceptualization: Neha Kumari; Methodology: Rajni Kant, Neha Kumari, Ruchika Sharma; Software: Neha Kumari; Synthesis (FTIR, ¹H NMR): Sandeep Ashok Sankpal, Archana Akaram Yadav; Formal Analysis: Rajni Kant; Investigation: Rajni Kant; Resources: Rajni Kant; Data Curation (Molecular docking): Saminathan Murugavel, Jayakumar Mohan Raj; Writing - Original Draft: Rajni Kant; Writing - Review and Editing: Rajni Kant; Visualization: Rajni Kant; Funding acquisition: Rajni Kant; Supervision: Rajni Kant; Project Administration: Rajni Kant.

ORCID and Email

Neha Kumari

 nehabhardwaj151995@gmail.com

 <https://orcid.org/0000-0003-4275-1390>

Ruchika Sharma

 ruchi18nik@gmail.com

 <https://orcid.org/0000-0002-5698-4067>

Archana Akaram Yadav

 yadavarchana743@gmail.com

 <https://orcid.org/0000-0003-2126-5967>

Sandeep Ashok Sankpal

 sandeeporg1@gmail.com

 <https://orcid.org/0000-0001-8209-5899>

Jayakumar Mohan Raj

 jmohanraj02@gmail.com

 <https://orcid.org/0000-0001-9765-0058>

Saminathan Murugavel

 smurugavel27@gmail.com

 <https://orcid.org/0000-0002-4626-8104>

Rajni Kant

 rkant.ju@gmail.com

 <http://orcid.org/0000-0001-8043-2329>

References

- Jain, Z. J.; Gide, P. S.; Kankate, R. S. Biphenyls and their derivatives as synthetically and pharmacologically important aromatic structural moieties. *Arab. J. Chem.* **2017**, *10*, S2051–S2066.
- Bridges, J. W.; Creaven, P. J.; Williams, R. T. The fluorescence of some biphenyl derivatives. *Biochem. J.* **1965**, *96*, 872–878.
- Yamamura, K.; Ono, S.; Tabushi, I. New liquid crystals having 4,4'-biphenanthryl core. *Tetrahedron Lett.* **1988**, *29*, 1797–1798.
- Hohnholz, D.; Schweikart, K.-H.; Subramanian, L. R.; Wedel, A.; Wischert, W.; Hanack, M. Synthesis and studies on luminescent biphenyl compounds. *Synth. Met.* **2000**, *110*, 141–152.
- Cincinelli, R.; Zwick, V.; Musso, L.; Zuco, V.; De Cesare, M.; Zunino, F.; Simoes-Pires, C.; Nurisso, A.; Giannini, G.; Cuendet, M.; Dallavalle, S. Biphenyl-4-yl-acrylohydroxamic acids: Identification of a novel indolyl-substituted HDAC inhibitor with antitumor activity. *Eur. J. Med. Chem.* **2016**, *112*, 99–105.
- Lee, C.-Y.; Choi, H.; Park, E.-Y.; Nguyen, T.-T.-L.; Maeng, H.-J.; Mee Lee, K.; Jun, H.-S.; Shin, D. Synthesis and anti-diabetic activity of novel biphenylsulfonamides as glucagon receptor antagonists. *Chem. Biol. Drug Des.* **2021**, *98*, 733–750.
- Pisano, M.; Dettori, M. A.; Fabbri, D.; Delogu, G.; Palmieri, G.; Rozzo, C. Anticancer activity of two novel hydroxylated biphenyl compounds toward malignant melanoma cells. *Int. J. Mol. Sci.* **2021**, *22*, 5636.
- Zhao, D.; Zhao, S.; Zhao, L.; Zhang, X.; Wei, P.; Liu, C.; Hao, C.; Sun, B.; Su, X.; Cheng, M. Discovery of biphenyl imidazole derivatives as potent antifungal agents: Design, synthesis, and structure-activity relationship studies. *Bioorg. Med. Chem.* **2017**, *25*, 750–758.
- Deep, A.; Jain, S.; Sharma, P. C. Synthesis and anti-inflammatory activity of some novel biphenyl-4-carboxylic acid 5-(arylidene)-2-(aryl)-4-oxothiazolidin-3-yl amides. *Acta Pol. Pharm.* **2010**, *67*, 63–67.
- Morawska, K.; Jedlińska, K.; Smarzewska, S.; Metelka, R.; Ciesielski, W.; Guziejewski, D. Analysis and DNA interaction of the profluralin herbicide. *Environ. Chem. Lett.* **2019**, *17*, 1359–1365.
- Ghatge, S.; Yang, Y.; Moon, S.; Song, W.-Y.; Kim, T.-Y.; Liu, K.-H.; Hur, H.-G. A novel pathway for initial biotransformation of dinitroaniline herbicide butralin from a newly isolated bacterium *Sphingopyxis* sp. strain HMH. *J. Hazard. Mater.* **2021**, *402*, 123510.
- Tavera-Hernández, R.; Jiménez-Estrada, M.; Alvarado-Sansininea, J. J.; Nieto-Camacho, A.; López-Muñoz, H.; Sánchez-Sánchez, L.; Escobar, M. L. Synthesis of chrysin, quercetin and naringin nitroderivatives: Antiproliferative, anti-inflammatory and antioxidant activity. *Let. Drug Des. Discov.* **2021**, *18*, 795–805.
- Ribeiro, T. A.; Machado-Ferreira, E.; Guimarães, L. F.; Cavaleiro, J.; Britto, A. M. A.; Redua, N.; de Souza, L. M. P.; Pimentel, A. S.; Picciani, P. H. S.; Oliveira, O. N., Jr; Barreto, C. B.; Soares, C. A. G. Novel cytotoxic amphiphilic nitro-compounds derived from a synthetic route for paraconic acids. *Colloids Surf. A Physicochem. Eng. Asp.* **2021**, *626*, 126984.
- Adedapo, A. D. A.; Ajayi, A. M.; Ekwunife, N. L.; Falayi, O. O.; Oyagbemi, A.; Omobowale, T. O.; Adedapo, A. A. Antihypertensive effect of *Phragmanthera incana* (Schum) Balle on NG-nitro-L-Arginine methyl ester (L-NAME) induced hypertensive rats. *J. Ethnopharmacol.* **2020**, *257*, 112888.
- Rice, A. M.; Long, Y.; King, S. B. Nitroaromatic antibiotics as nitrogen oxide sources. *Biomolecules* **2021**, *11*, 267.
- Becker, F. F.; Mukhopadhyay, C.; Hackfeld, L.; Banik, I.; Banik, B. K. Polycyclic aromatic compounds as anticancer agents: synthesis and biological evaluation of dibenzofluorene derivatives. *Bioorg. Med. Chem.* **2000**, *8*, 2693–2699.
- Bisel, P.; Al-Momani, L.; Müller, M. The *tert*-butyl group in chemistry and biology. *Org. Biomol. Chem.* **2008**, *6*, 2655–2665.
- Chkirate, K.; Akachar, J.; Hni, B.; Hökelek, T.; Anouar, E. H.; Talbaoui, A.; Mague, J. T.; Sebbar, N. K.; Ibrahim, A.; Essassi, E. M. Synthesis,

- spectroscopic characterization, crystal structure, DFT, ESI-MS studies, molecular docking and in vitro antibacterial activity of 1,5-benzodiazepin-2-one derivatives. *J. Mol. Struct.* **2022**, *1247*, 131188.
- [19]. Carvalho, A. J. P.; Dordio, A. V.; Ramalho, J. P. P. A DFT study on the adsorption of benzodiazepines to vermiculite surfaces. *J. Mol. Model.* **2014**, *20*, 2336.
- [20]. Hok, L.; Božičević, L.; Sremec, H.; Šakić, D.; Vrček, V. Racemization of oxazepam and chiral 1,4-benzodiazepines. DFT study of the reaction mechanism in aqueous solution. *Org. Biomol. Chem.* **2019**, *17*, 1471–1479.
- [21]. Ganjali Koli, M.; Azizi, K. Investigation of benzodiazepines (BZDs) in a DPPC lipid bilayer: Insights from molecular dynamics simulation and DFT calculations. *J. Mol. Graph. Model.* **2019**, *90*, 171–179.
- [22]. McClendon, A. K.; Osherooff, N. DNA topoisomerase II, genotoxicity, and cancer. *Mutat. Res.* **2007**, *623*, 83–97.
- [23]. Gibson, E. G.; Bax, B.; Chan, P. F.; Osherooff, N. Mechanistic and structural basis for the actions of the antibacterial gepotidacin against *Staphylococcus aureus* gyrase. *ACS Infect. Dis.* **2019**, *5*, 570–581.
- [24]. Sheldrick, G. M. A short history of SHELX. *Acta Crystallogr. A* **2008**, *64*, 112–122.
- [25]. Sheldrick, G. M. SHELXT - integrated space-group and crystal-structure determination. *Acta Crystallogr. A Found. Adv.* **2015**, *71*, 3–8.
- [26]. Dolomanov, O. V.; Bourhis, L. J.; Gildea, R. J.; Howard, J. A. K.; Puschmann, H. OLEX2: a complete structure solution, refinement and analysis program. *J. Appl. Crystallogr.* **2009**, *42*, 339–341.
- [27]. Spek, A. L. Structure validation in chemical crystallography. *Acta Crystallogr. D Biol. Crystallogr.* **2009**, *65*, 148–155.
- [28]. Nardelli, M. Parst: A system of fortran routines for calculating molecular structure parameters from results of crystal structure analyses. *Comput. Chem.* **1983**, *7*, 95–98.
- [29]. Macrae, C. F.; Bruno, I. J.; Chisholm, J. A.; Edgington, P. R.; McCabe, P.; Pidcock, E.; Rodriguez-Monge, L.; Taylor, R.; van de Streek, J.; Wood, P. A. Mercury CSD 2.0– new features for the visualization and investigation of crystal structures. *J. Appl. Crystallogr.* **2008**, *41*, 466–470.
- [30]. Lee, C.; Yang, W.; Parr, R. G. Development of the Colle-Salvetti correlation-energy formula into a functional of the electron density. *Phys. Rev. B Condens. Matter* **1988**, *37*, 785–789.
- [31]. Frisch, M. J.; Trucks, G. W.; Schlegel, H. B.; Scuseria, G. E.; Robb, M. A.; Cheeseman, J. R.; Montgomery, J. A.; Vreven, T.; Kudin, K. N.; Burant, J. C.; Millam, J. M.; Iyengar, S. S.; Tomasi, J.; Barone, V.; Mennucci, B.; Cossi, M.; Scalmani, G.; Rega, N.; Petersson, G. A.; Nakatsuji, H.; Hada, M.; Ehara, M.; Toyota, K.; Fukuda, R.; Hasegawa, J.; Ishida, M.; Nakajima, T.; Honda, Y.; Kitao, O.; Nakai, H.; Klene, M.; Li, X.; Knox, J. E.; Hratchian, H. P.; Cross, J. B.; Adamo, C.; Jaramillo, J.; Gomperts, R.; Stratmann, R. E.; Yazyev, O.; Austin, A. J.; Cammi, R.; Pomelli, C.; Ochterski, J. W.; Ayala, P. Y.; Morokuma, K.; Voth, G. A.; Salvador, P.; Dannenberg, J. J.; Zakrzewski, V. G.; Dapprich, S.; Daniels, A. D.; Strain, M. C.; Farkas, O.; Malick, D. K.; Rabuck, A. D.; Raghavachari, K.; Foresman, J. B.; Ortiz, J. V.; Cui, Q.; Baboul, A. G.; Clifford, S.; Cioslowski, J.; Stefanov, B. B.; Liu, G.; Liashenko, A.; Piskorz, P.; Komaromi, I.; Martin, R. L.; Fox, D. J.; Keith, T.; Al-Laham, M. A.; Peng, C. Y.; Nanayakkara, A.; Challacombe, M.; Gill, P. M. W.; Johnson, B.; Chen, W.; Wong, M. W.; Gonzalez, C.; Pople, J. A. Gaussian 09, rev. A.01, Gaussian Inc., Wallingford CT, 2013.
- [32]. Dennington, R.; Keith, T. A.; Millam, J. M. GaussView, Version 6, Semichem Inc.; Shawnee Mission, KS, 2016.
- [33]. Spackman, P. R.; Turner, M. J.; McKinnon, J. J.; Wolff, S. K.; Grimwood, D. J.; Jayatilaka, D.; Spackman, M. A. CrystalExplorer: a program for Hirshfeld surface analysis, visualization and quantitative analysis of molecular crystals. *J. Appl. Crystallogr.* **2021**, *54*, 1006–1011.
- [34]. Morris, G. M.; Huey, R.; Lindstrom, W.; Sanner, M. F.; Belew, R. K.; Goodsell, D. S.; Olson, A. J. AutoDock4 and AutoDockTools4: Automated docking with selective receptor flexibility. *J. Comput. Chem.* **2009**, *30*, 2785–2791.
- [35]. Pai, E. F.; Krengel, U.; Petsko, G. A.; Goody, R. S.; Kabsch, W.; Wittinghofer, A. Refined crystal structure of the triphosphate conformation of H-ras p21 at 1.35 Å resolution: implications for the mechanism of GTP hydrolysis. *EMBO J.* **1990**, *9*, 2351–2359.
- [36]. Dassault Systèmes BIOVIA, BIOVIA Workbook, Release 2021; BIOVIA DS Visualizer, Release 2021, San Diego: Dassault Systèmes, 2021. <https://discover.3ds.com/discovery-studio-visualizer-download> (accessed 2022-05-14).
- [37]. Rajnikant; Gupta, V. K.; Kumar, A.; Bamezai, R. K.; Sharma, N. K. Crystallography of 4,4-bis-(n-propylamino)-biphenyl [C18N2H24]. *Mol. Cryst. Liq. Cryst.* **1999**, *333*, 237–242.
- [38]. Rajnikant; Dinesh; Singh, D. X-ray structure determination and analysis of hydrogen interactions in 3,3'-dimethoxybiphenyl. *Bull. Mater. Sci. (India)* **2004**, *27*, 31–34.
- [39]. Dhankhar, J.; González-Fernández, E.; Dong, C.-C.; Mukhopadhyay, T. K.; Linden, A.; Čorić, I. Spatial anion control on palladium for mild C-H arylation of Arenes. *J. Am. Chem. Soc.* **2020**, *142*, 19040–19046.
- [40]. Sharif, M.; Zeeshan, M.; Reimann, S.; Villinger, A.; Langer, P. One-pot synthesis of fluorinated terphenyls by site-selective Suzuki-Miyaura reactions of 1,4-dibromo-2-fluorobenzene. *Tetrahedron Lett.* **2010**, *51*, 2810–2812.
- [41]. Zazouli, S.; Láallam, L.; Ketatni, E. M. Synthesis of novel benzohydrazide and benzoic acid derivatives: Crystal Structure, Hirshfeld surface analysis and DFT computational studies. *J. Mol. Struct.* **2021**, *1239*, 130465.
- [42]. Aihara, J.-I. Weighted HOMO-LUMO energy separation as an index of kinetic stability for fullerenes. *Theor. Chem. Acc.* **1999**, *102*, 134–138.
- [43]. Sallam, H. H.; Mohammed, Y. H. E.; Al-Ostoot, F. H.; Sridhar, M. A.; Khanum, S. A. Synthesis, structure analysis, DFT calculations, Hirshfeld surface studies, and energy frameworks of 6-Chloro-3-[[4-chloro-3-methylphenoxy)methyl][1,2,4]triazolo[4,3-b]pyridazine. *J. Mol. Struct.* **2021**, *1237*, 130282.
- [44]. Manne, R.; Åberg, T. Koopmans' theorem for inner-shell ionization. *Chem. Phys. Lett.* **1970**, *7*, 282–284.
- [45]. Priya, M. K.; Revathi, B. K.; Renuka, V.; Sathya, S.; Asirvatham, P. S. Molecular structure, spectroscopic (FT-IR, FT-Raman, 13C and 1H NMR) analysis, HOMO-LUMO energies, Mulliken, MEP and thermal properties of new chalcone derivative by DFT calculation. *Mater. Today* **2019**, *8*, 37–46.
- [46]. Somagond, S. M.; Wari, M. N.; Shaikh, S. K. J.; Inamdar, S. R.; Shankar, M. K.; Prasad, D. J.; Kamble, R. R. Detailed analytical studies of 1,2,4-triazole derivatized quinoline. *Eur. J. Chem.* **2019**, *10*, 281–294.
- [47]. Moro, S.; Bacilieri, M.; Ferrari, C.; Spalluto, G. Autocorrelation of molecular electrostatic potential surface properties combined with partial least squares analysis as alternative attractive tool to generate ligand-based 3D-QSARs. *Curr. Drug Discov. Technol.* **2005**, *2*, 13–21.
- [48]. Mathammal, R.; Sangeetha, K.; Sangeetha, M.; Mekala, R.; Gadheja, S. Molecular structure, vibrational, UV, NMR, HOMO-LUMO, MEP, NLO, NBO analysis of 3,5-di-tert-butyl 4-hydroxy benzoic acid. *J. Mol. Struct.* **2016**, *1120*, 1–14.
- [49]. Spackman, M. A.; McKinnon, J. J. Fingerprinting intermolecular interactions in molecular crystals. *CrystEngComm* **2002**, *4*, 378–392.
- [50]. Singh, M.; Anthal, S.; Srijana, P. J.; Narayana, B.; Sarojini, B. K.; Likhitha, U.; Kamal; Kant, R. Novel supramolecular co-crystal of 3-aminobenzoic acid with 4-acetyl-pyridine: Synthesis, X-ray structure, DFT and Hirshfeld surface analysis. *J. Mol. Struct.* **2022**, *1262*, 133061.



Copyright © 2023 by Authors. This work is published and licensed by Atlanta Publishing House LLC, Atlanta, GA, USA. The full terms of this license are available at <http://www.eurjchem.com/index.php/eurjchem/pages/view/terms> and incorporate the Creative Commons Attribution-Non Commercial (CC BY NC) (International, v4.0) License (<http://creativecommons.org/licenses/by-nc/4.0>). By accessing the work, you hereby accept the Terms. This is an open access article distributed under the terms and conditions of the CC BY NC License, which permits unrestricted non-commercial use, distribution, and reproduction in any medium, provided the original work is properly cited without any further permission from Atlanta Publishing House LLC (European Journal of Chemistry). No use, distribution, or reproduction is permitted which does not comply with these terms. Permissions for commercial use of this work beyond the scope of the License (<http://www.eurjchem.com/index.php/eurjchem/pages/view/terms>) are administered by Atlanta Publishing House LLC (European Journal of Chemistry).